Pairs of Solitons Bound by Noise-Mediated Casimir-Like Interactions

Kfir Sulimany[1,*], Offek Tziperman[1,*], Yaron Bromberg[1], and Omri Gat[1,2]

[1]Racah Institute of Physics, The Hebrew University of Jerusalem, Jerusalem 91904, Israel
[*]The first two authors have equal contribution.
[2]Corresponding author: omrigat@mail.huji.ac.il

Abstract

We study experimentally and theoretically the steady states of two-soliton waveforms that form stationary bound states in a fiber laser, passively mode locked by a nonlinear-multimode-interference-based saturable absorber. We control the steady state separation by changing the laser parameters, and in particular demonstrate a dynamical transition between loosely-bound states where the the solitons interact via the noise-mediated Casimir-like interactions, and tightly-bound states dominated by coherent overlap interactions. We show that the measured pulse separations of the loosely bound pairs are well-described by the NMI theory, and present a steady state phase diagram that captures the transitions between the loosely- and tightly-bound states as an intrinsic consequence of the form of the noise-mediated interaction effective potential.

1 Introduction

Dissipative solitons are localized waves in open systems far from equilibrium, whose existence result from a balance of dissipative and dispersive effects. They appear in numerous physical areas including reaction-diffusion systems, neurological and ecological sciences, fluid dynamics, and photonics [1–7]. Photonics is a great platform to observe the nonlinear complex behavior of dissipative solitons [8–14]. In particular, collective nonlinear phenomena such as the aggregation of solitons into bunches have created great interest [15–28].

Multi-soliton patterns exhibit an extensive pallet of short and long-range pulse interactions. Short-range interactions take place when pulse tails overlap [21,29–32]. However, interactions over separations of orders of magnitude beyond the width of individual solitons must be mediated by the the gain [19,33], or by acoustic response [17,34,35]. Furthermore, non-soliton components of optical pulses, such as dispersive-wave pedestals give rise to interactions with an intermediate range significantly longer than the soliton width, but much shorter than the cavity length [18,36]. Recently, the transition between complex soliton states has been achieved utilizing optical modulation components [35,37,38]. However, a model that captures the dynamics of both coherently coupled and incoherently coupled solitons is still lacking.

Recently, we introduced a long-range interaction mechanism arising from the effect of gain depletion in the presence of noisy quasi-CW light in a mode-locked laser [33,39]. The interaction results from the reduction of optical fluctuations due to gain depletion, following the passage of a pulse through the gain medium. Suppression of fluctuations decreases the temporal jitter of subsequent pulses and in this way biases the jitter and sets the pulse motion. This noise-mediated interaction (NMI) mechanism shares some intriguing properties with the Casimir effect in quantum electrodynamics, where macroscopic objects experience an effective interaction due to suppression of electromagnetic field fluctuations [40]. In both the NMI and the Casimir effect, distant objects inhibit microscopic fluctuations in extended electromagnetic modes. The consequent breaking of spatiotemporal homogeneity gives rise to the weak interactions among these objects.

Optical solitons in anomalous-dispersion mode-locked lasers are often accompanied by weak and broad dispaerswave pedestals [41]. When solitons are well-separated, the NMI is generally attractive [33], but when two solitons are close enough that their pedestals overlap, the interaction can become repulsive; consequently NMI can lead to the formation of bound states of solitons whose steady-state separation is comparable with the pedestal width. The overall phases of solitons in such bound states are not coherently locked, so that they can be viewed as *loosely bound*.

The propagation of dispersive waves in a mode-locked laser is highly sensitive to the overall net gain, which means that the pedestals can be controlled by the amplifier pump. Here, we use this control knob to experimentally observe and manipulate the steady state of a two-pulse waveform in an all-fiber laser that is passively mode-locked. Satuable absorption is achieved by a nonlinear multimode interference [42]. The NMI theory makes precise predictions about the dependence of the pulse separation on the pedestal power and width, which are in quantitative agreement with the experimental measurements, demonstrating that NMI is the

dominant mechanism in long-range pulse interactions in mode-locked fiber lasers of this type.

Even though, as explained, the pedestal overlap induces effective inter-pulse repulsion, repulsion is strong enough to generate a loosely bound state only for a large enough pedestal power. Our experiments confirm this theoretical prediction, and demonstrate a transition to a state with *tightly bound* solitons with locked phases, below the pedestal power threshold. The controllability of the pulse separation and the ability to switch from loosely- to tightly-bound soliton regime, constitute a significant step toward applications of multipulse laser waveforms.

2 Results

2.1 Mode-Locked Fiber Laser

The mode-loked laser is based on an all-fiber integrated ring cavity operated in the anomalous dispersion regime [43]. The cavity length is 14m, including a 2.7m erbium-doped fiber gain medium, as depicted in Figure 1. The erbium-doped fiber is core pumped by a 976 nm diode laser through a wavelength-division multiplexer. A polarization-independent optical isolator ensures unidirectional lasing and two fiber polarization controllers tune the overall low cavity birefringence. Finally, a 90/10 coupler provides the laser output.

The mode-locking operation is passively achieved by employing a nonlinear multimode interference-based saturable absorber [44–51]. In this scheme, light occupying a single spatial mode is coupled to a multimode fiber (MMF), whose output facet is spliced to a single mode fiber as depicted in Figure 1. The intensity at the splicing point depends on the interference of the excited MMF modes. At high power, the interference is modified by Kerr nonlinearity making the transmittance at the splicing point power-dependent. In our setup, we utilize a 1.5 m long segment of graded-index multimode fiber (OM1; 62.5 μm core diameter, NA = 0.275) adopted as an effective saturable absorber. This design allows us to modify the absorber properties, such as linear loss, saturated loss, and saturation power, by adjusting the MMF position and the polarization controller. As a result, a wider range of soliton configurations can be achieved [52]. The laser output was analyzed with an optical spectrum analyzer (Yokagawa AQ6374), and a fast photodiode connected to a real-time oscilloscope (Tektronix MSO70804C).

We produce stationary patterns of soliton pairs by varying the pump power beyond the threshold for stable single-pulse operation. The laser output spectrum is presented in Figure 2(a) as a function of the pumping current. The central wavelength is 1561 nm, and the full width at half maximum bandwidth is ∼3.8 nm. At pumping currents below 120 mA, we observe spectral fringes
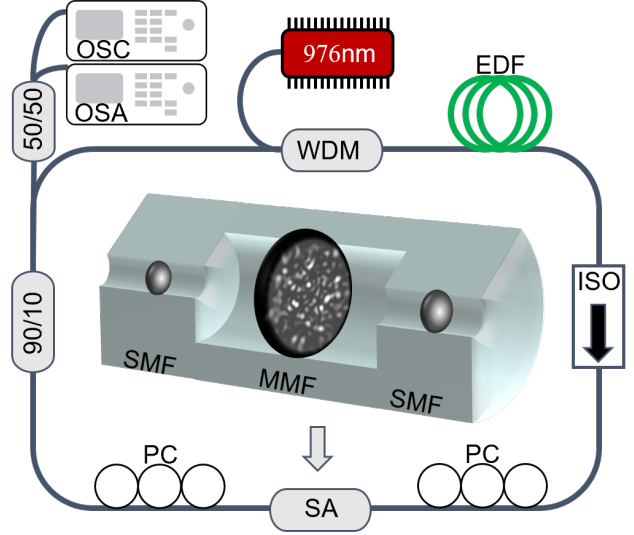

Figure 1: SA: saturable absorber, SMF: single mode fiber, MMF: multimode fiber, EDF: erbium-doped fiber, WDM: wavelength-division multiplexer, ISO: optical isolator, PC: polarization controller, OSA: optical spectrum analyzer, OSC: oscilloscope.

indicating that the solitons interact coherently, so that their phases are locked, i.e the solitons tightly bound; at higher pumping currents there are no interference fringes, so that the pulse phases are not coherently locked, which means that the solitons are loosely bound.

Narrow sidebands appear at the primary Gordon-Kelly resonances [53, 54], 1553 nm and 1567 nm, and their power grows with the pumping current. Figure 2(c) presents two spectral cross-sections of Figure 2(a), at pumping currents of 123 mA (blue) and 120 mA (red), exhibiting the Kelly sidebands and the interference fringes in the latter.

Figure 2(b) presents time domain traces of the cavity waveform intensity as a function of the pumping current, where two maxima are observed at high enough pumping currents, above 121 mA. At lower pumping currents the soliton separation is too small to be resolved in the oscilloscope, but the approximate conservation of total energy in the soliton waveform shows that the number of solitons has not changed. Indeed, the time-domain cross sections at pumping currents of 123 mA (blue) and 120 mA (red) presented in Figure 2(d), imply that both waveforms have equal total energy, proportional to the total area under the curves, as expected from the clamping of the soliton energy in anomalous-dispersion passively mode-locked lasers [55–57]. Below 120 mA in particular, the separation time is estimated from the spectral interference pattern at a few ps, far below the electronic resolution of the 8 GHz bandwidth of the oscilloscope.
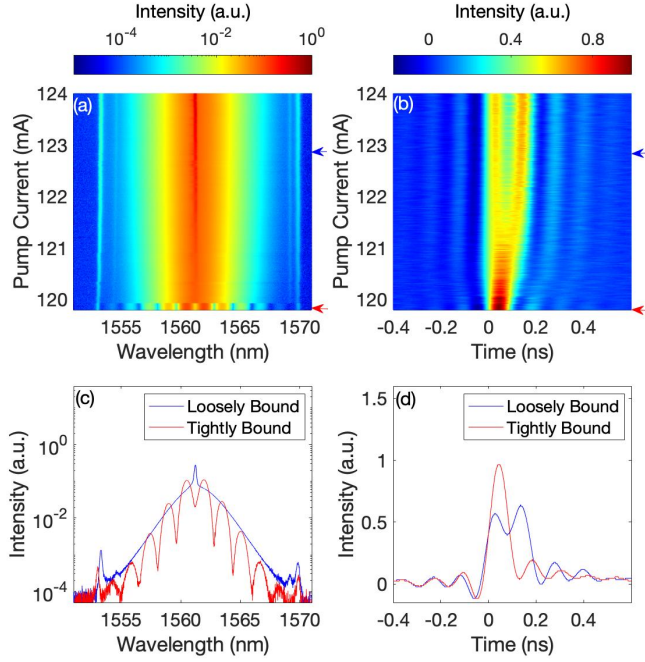
Figure 2: (a) The laser's output spectrum measured as a function of the pumping current. Cross sections at pumping powers of 123 mA (blue arrows) and 120 mA (red arrows) plotted in (c) demonstrate the two soliton binding regimes; Loosely bound (LB) pairs with fluctuating relative phase and Tightly bound (TB) pairs with coherently locked phases. (b) The lasers temporal profile measured as a function of the pumping current using a fast photo detector. (d) Cross sections at pumping currents of 123 mA (blue arrows) and 120 mA (red arrows) plotted in (d) demonstrate that the total energy in the soliton waveform remains nearly constant even when the inter-soliton separation is too small to be resolved by the oscilloscope.

2.2 Noise-Mediated Soliton Interaction

The NMI mechanism was first proposed in [33], together with the basic equations of motion governing the pulse motion. The interaction is based on fluctuations of pulse timing generated by overlap with the quasi-CW permeating the cavity, and is mediated by the gain dynamics, and is therefore expected to work in any multi-pulse mode locked laser, although its importance compared with other interaction mechanism can vary widely between different systems. We briefly explain the principles of NMI with an emphasis on the aspects relevant to the present work, and refer the reader to [33] for more details.

We approximate the the laser waveform form as the incoherent sum of n non-overlapping soliton waveforms centered at time points t_n (in the frame moving with the group velocity of a single soliton), each of which is accompanied by a weak and broad dispersive-wave pedestal generated by the Gordon-Kelly resonances [41], and an extended quasi-CW waveform; the quasi-CW is generated by noise buildup, and therefore has random phase, as indicated in Figure 3. The growth of the quasi-CW is limited by the small signal net loss, and therefore the quasi-CW intensity is inversely proportional to the net loss in a uniform system. However, since the amplifier gain is depleted by the passage of a pulse, and gain recovery is slow, the gain profile $g(t)$ is nonuniform, which means that the quasi-CW intensity is not uniform either.

The gain profile is governed by the differential equation

$$\frac{dg}{dt} = g_r - g_s \sum_k I_p(t - t_k) , \qquad (1)$$

where g_r and g_s are the gain recovery and gain saturation coefficients, respectively, and $I_p(t)$ is the intensity profile of a pulse centered at zero. We approximate g_r by a constant because the recovery time of gain media typically used in mode locked fiber laser is typically much longer than the roundtrip time [58]. As explained, the pulse intensity profile has two components: The soliton component is approximated by a delta function because it is much shorter than all other time scales, and the pedestal component, is modeled with an exponential decaying on time scale w that is much longer than the pulse width but much shorter than the cavity roundtrip time t_R,

$$I_p(t) = E_s \delta(t) + \frac{E_p}{2w} e^{-|t|/w} , \qquad (2)$$

E_s, E_p being the pulse and pedestal energy, respectively. Consequently, the gain profile $g(t)$ is a smoothed-corner sawtooth shaped function, as shown in Figure 3, together the pulse-intensity profile. Note that the gain recovery rate g_r, which is fixed in Equation 1 by continuity and the total pulse energy, sets the saturation depth of the gain.

The overlap of a pulse and the noisy continuum is a source of timing jitter [59, 60], which can be modeled as a diffusion process, where the diffusion coefficient D_k of pulse number k is proportional to the instantaneous quasi-CW power, at time t_k, which is determined by the net gain profile as [33],

$$D_k \propto (\frac{1}{\sqrt{l - g_k^-}} + \frac{1}{\sqrt{l - g_k^+}}) \qquad (3)$$

where l is the total small signal loss and g_k^-, g_k^+ are the values of the gain coefficient just before and just after the kth pulse, respectively. Note that the D_k depend on the pulse separations, since the separations determine the gain profile. consequently, the pulse jitter is biased even though the noise itself is symmetrically distributed, with an effective drift

$$\frac{d\langle t_k \rangle}{dz} = \frac{1}{2} \frac{\partial D_k}{\partial t_k} \qquad (4)$$
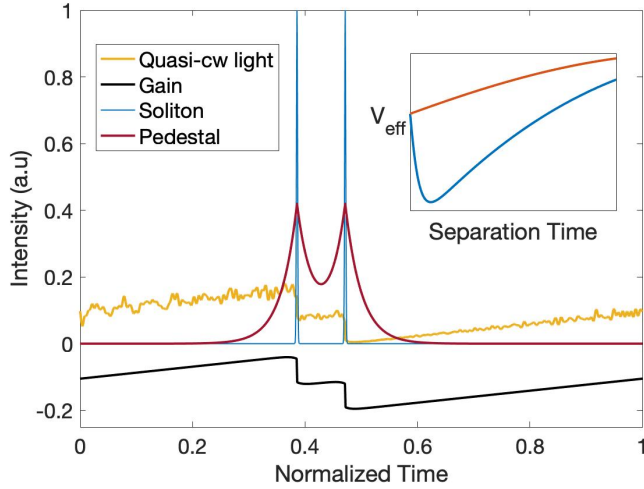
Figure 3: **Illustration of the NMI mechanism.**
Passage of soliton pulses through the gain medium depletes the instantaneous gain. A pair of pulses yields a smoothed saw-tooth gain profile. The quasi-CW light light that runs in the cavity is determined by the gain profile, and thus also exhibits a smoothed saw-tooth profile. The NMI is a by-product of the pulse timing jitter caused by nonlinear interaction between the pulses and the quasi-CW light. The inset shows the effective potential for the noise-mediated interaction of the loosely bound (blue) and tightly bound (red) states.

where the brackets indicate noise-averaging.

From this point we consider two-soliton waveforms; the drift equations (Equation 4) can be expressed as over-damped motion in an effective potential [33] that is attractive at large separations, but may have a minimum at a separation value t_s of the order of the pedestal width, corresponding to a stable loosely bound state at this separation (see inset of Figure 3). The pedestal width is much smaller than the cavity roundtrip time, and in this limit

$$\tilde{t}_s = \tilde{w}\ln(\frac{\tilde{E}_p}{\tilde{w}}) , \qquad \text{if } \tilde{E}_p > \tilde{w} \qquad (5)$$

where $\tilde{t}_s = t_s/t_R$, $\tilde{w} = w/t_R$, and $\tilde{E}_p = E_p/(E_s + E_p)$; if $\tilde{E}_p < \tilde{w}$, on the other hand, the minimum of the effective inter-pulse potential appears at zero separation time, so that the noise-mediated interaction causes attraction at all separations.

When the pulse separation is very small, comparable with the soliton width, coherent overlap interaction becomes appreciable, and at some point dominates over the NMI, and then the phases of the two pulses lock, and they become tightly bound. The transition between the NMI and coherent-overlap interaction is not well understood at the moment; our experiments find that pulses spaced by 10ps or less are tightly bound.

2.3 Soliton Steady States Analysis

We extract from Figure 2(a-b) and from six other datasets the separation times between the pulses, and the Kelly-sidebands energies, which are equal to the pedestal energy. In Figure 4(a) we present the separation times of the soliton pairs, normalized by the cavity round trip time, versus the pedestal energy, normalized by the pulse energy. The dots and triangles correspond to data measured at the loosely bound (LB), and at the tightly bound (TB) regimes, respectively. Each mark represents the mean of ten consecutive measurements with the error-bars corresponding to the standard deviation. The seven different datasets are obtained for different configurations of the polarization controllers that modify the SA behavior. The (almost straight) curves in Figure 4(a) correspond to the NMI prediction (Equation 5), with a constant pedestal width as a fit parameter, showing a good agreement with the experimental results. The fit assumed pedestal widths w of 42 ps, 47 ps, 70 ps, 77 ps, 77 ps, 84 ps, 98 ps (corresponding to normalized widths $\tilde{w}$ of $0.6 \cdot 10^{-3}, 0.67 \cdot 10^{-3}, 1 \cdot 10^{-3}, 1.1 \cdot 10^{-3}, 1.1 \cdot 10^{-3}, 1.2 \cdot 10^{-3}, 1.4 \cdot 10^{-3}$, respectively) for datasets 1–7, respectively. While we could not measure the pedestal widths directly using the oscilloscope, we obtained a lower bound of $10ps$ for the widths (corresponding to a lower bound of $0.14 \cdot 10^{-3}$ for the normalized widths) by Fourier transform of the widest Lorentzian shaped Kelly sideband measured (corresponding to the narrowest pedestals in the time domain) [41]. We note that the lower bound is not sharp, because it does not take into account the broadening of the measured Kelly sidebands due to the $50pm$ resolution of the optical spectrum analyzer. Another source of apparent broadening of the sidebands is that the Gordon-Kelly resonant wavelengths of the two pulses are slightly different, because of the slight difference in their powers.

We next propose an approach to observe the transition between loosely and tightly bound steady states by adjusting the pumping current. By decreasing the pumping current, we decrease the normalized pedestal energy. According to Equation 5, the pulse separation time decreases with the normalized pedestal energy. As the pumping current is decreased, therefore, two scenarios may occur. The first scenario is that the separation time decreases down until it becomes comparable with the soliton width. In this scenario, a dynamical transition occurs and the pulse separation, together with their relative phase, are locked by the coherent overlap interaction, as explained in the previous section. This is the transition between loosely and tightly bound soliton pairs observed in datasets 3 and 5 in Figure 4(b). Note that the transition is made by tuning only the pumping current without any additional intervention.
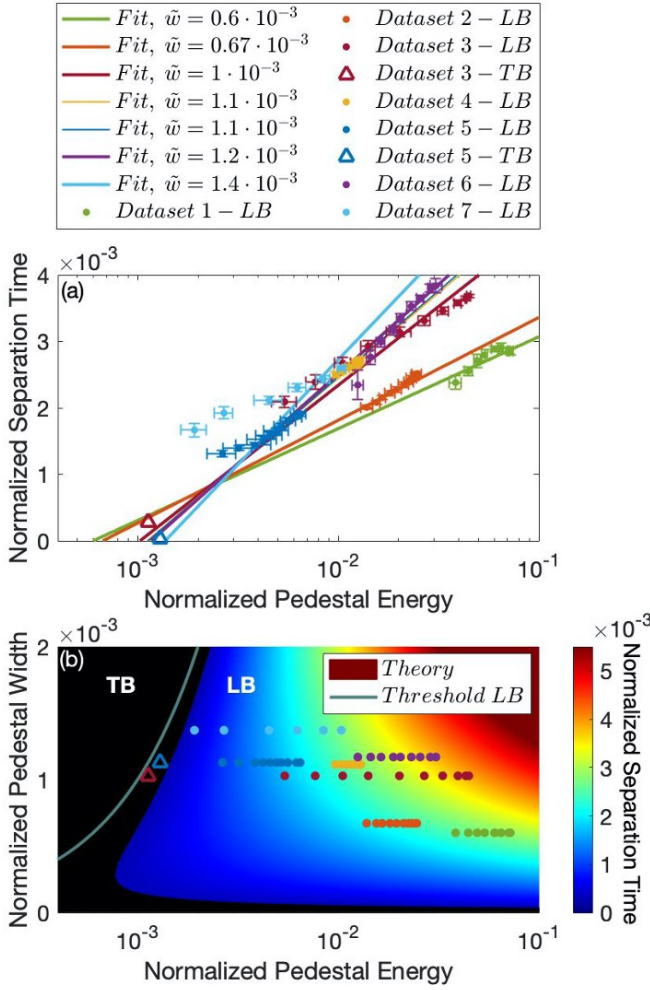
Figure 4: **Soliton steady states analysis.** (a) The measured separation time of the soliton pair, normalized by the cavity round trip time, versus the pedestal energy, normalized by the pulse energy. Seven different data sets obtained by adjusting the polarization controllers to modify the nonlinear interference in the MMF and thus change the SA properties. The NMI theory (solid line) agrees with the experimental data in the loosely bound (LB) regime and the tightly bound (TB) regime. (b) Theoretically predicted stable separation time for the two pulse loosely bound state plotted as a function of normalized pedestal width and normalized pedestal energy. The green line indicates the threshold for a loosely bound state at a non-zero separation time. The black area marks separation times smaller than $0.14 \cdot 10^{-3}$, in scale of the soliton duration, in these areas, the NMI is weak comparing to the coherent interaction. Therefore, a phase transition occurs between the loosely and tightly bound states. The experimental results are marked by dots (loosely bound) and triangles (tightly bound). The pedestal energy and width are normalized by the total pulse energy, and the cavity round trip time respectively. The dots correspond to the measured steady states presented in panel (a).

The second scenario that may occur when decreasing the pumping current is that the soliton pair state becomes unstable to pulse annihilation before we reach the threshold for the transition between the loosely and tightly bound states. This scenario is displayed by datasets 1, 2, 4, 6 and 7 in Figure 4(b), where the transition between loosely and tightly bound pairs cannot be reached. The switching between the two scenarios was achieved by adjusting the polarization controller to get different pedestal energies. The saturable absorber properties, such as small-signal loss, saturation power and transmission modulation, are sensitive to the polarization, and these properties determine the ratio between the pedestal energy and the soliton energy. Therefore by adjusting the polarization controller we can observe both scenarios in the cavity. In our system the second scenario is more common, while the first scenario is obtained only for the smallest of the observed pedestal energies.

3 Conclusions

This paper presents a quantitative study of stationary two-soliton waveforms in a mode locked laser, in which the pulse separation time is governed by the long-rage noise-mediated interaction (NMI) mechanism. In this loosely bound pair regime, where the separation between the pulses ranges from a few tens to a few hundred picoseconds, the soliton phases are not coherently locked, and the steady-state separation is determined by the dispersive-wave pedestal of the solitons. We show that for a fixed saturable absorber configuration, the joint variations of pedestal energy and the separation as a function of pump power is consistent the theoretical NMI prediction under the assumption of a fixed pedestal width as a fit parameter; the width could not be directly measured, but the fit values are consistent with indirect lower bounds.

In general, the pedestal energy is a monotonically increasing function of pumping current, and this implies by the NMI theory that separation is also an increasing function of the pumping current. Furthermore, the NMI theory predicts that as the pedestal energy decreases, the separation time drops to zero at a finite value of the pedestal energy. When this happens, the solitons become tightly bound, so that their relative phases of the pulses are locked and their separation is fixed by the coherent overlap interaction. By changing the saturable absorber properties we can switch between a pedestal energy range where the transition between loosely- and tightly-bound steady states is observed when pumping current is decreased, and a range where the waveform becomes unstable to pulse annihilation while the pulses are still loosely bound. In this way the NMI provides a systematic way to control the separation between the pulses in two-pulse mode-locked laser configuration, and in particular the transition between loosely- and tightly-

bound configurations.

In these experiments we controlled the pedestal energy and width using the pumping current and polarization controllers, and in this way indirectly manipulated the pulse steady states. We note it is possible instead to directly modify the pedestal waveform by introducing a spectral filter into the laser cavity, and in this way manipulate the pulse separation without modifying any of the laser parameters. Our experiments that demonstrate flexible and predictable control of the two pulse waveform should therefore be viewed also as a step forward toward the goal of synthesis and shaping of complex multi-soliton waveforms in mode locked lasers.

References

[1] H-G Purwins, HU Bödeker, and Sh Amiranashvili. Dissipative solitons. *Advances in Physics*, 59(5):485–701, 2010.

[2] Neil Akhmediev and Adrian Ankiewicz. Dissipative solitons in the complex ginzburg-landau and swift-hohenberg equations. In *Dissipative solitons*, pages 1–17. Springer, 2005.

[3] Andreas Liehr. *Dissipative solitons in reaction diffusion systems*. Springer, 2013.

[4] Philippe Grelu and Nail Akhmediev. Dissipative solitons for mode-locked lasers. *Nature photonics*, 6(2):84–92, 2012.

[5] Philippe Grelu. *Nonlinear optical cavity dynamics: from microresonators to fiber lasers*. John Wiley & Sons, 2015.

[6] Yufeng Song, Xujie Shi, Chengfa Wu, Dingyuan Tang, and Han Zhang. Recent progress of study on optical solitons in fiber lasers. *Applied Physics Reviews*, 6(2):021313, 2019.

[7] J Javaloyes, P Camelin, M Marconi, and M Giudici. Dynamics of localized structures in systems with broken parity symmetry. *Physical review letters*, 116(13):133901, 2016.

[8] Piotr Ryczkowski, M Närhi, Cyril Billet, J-M Merolla, Goëry Genty, and John Michaël Dudley. Real-time full-field characterization of transient dissipative soliton dynamics in a mode-locked laser. *Nature Photonics*, 12(4):221–227, 2018.

[9] Xueming Liu and Meng Pang. Revealing the buildup dynamics of harmonic mode-locking states in ultrafast lasers. *Laser & Photonics Reviews*, 13(9):1800333, 2019.

[10] Xueming Liu, Daniel Popa, and Nail Akhmediev. Revealing the transition dynamics from q switching to mode locking in a soliton laser. *Physical review letters*, 123(9):093901, 2019.

[11] Junsong Peng and Heping Zeng. Soliton collision induced explosions in a mode-locked fibre laser. *Communications Physics*, 2(1):1–8, 2019.

[12] Qiu-Yi Ning, Hao Liu, Xu-Wu Zheng, Wei Yu, Ai-Ping Luo, Xu-Guang Huang, Zhi-Chao Luo, Wen-Cheng Xu, Shan-Hui Xu, and Zhong-Min Yang. Vector nature of multi-soliton patterns in a passively mode-locked figure-eight fiber laser. *Optics express*, 22(10):11900–11911, 2014.

[13] Zhenhong Wang, Zhi Wang, Yange Liu, Ruijing He, Jian Zhao, Guangdou Wang, and Guang Yang. Self-organized compound pattern and pulsation of dissipative solitons in a passively mode-locked fiber laser. *Optics letters*, 43(3):478–481, 2018.

[14] Mathias Marconi, Julien Javaloyes, Salvador Balle, and Massimo Giudici. How lasing localized structures evolve out of passive mode locking. *Physical review letters*, 112(22):223901, 2014.

[15] D. J. Richardson, R. I. Laming, D. N. Payne, M. W. Phillips, and V. J. Matsas. 320 fs soliton generation with passively mode-locked erbium fibre laser. *Electronics Letters*, 27(9):730–732, April 1991.

[16] A. B. Grudinin, D. J. Richardson, and D. N. Payne. Passive harmonic modelocking of a fibre soliton ring laser. *Electronics Letters*, 29(21):1860–1861, October 1993.

[17] AN Pilipetskii, EA Golovchenko, and CR Menyuk. Acoustic effect in passively mode-locked fiber ring lasers. *Optics letters*, 20(8):907–909, 1995.

[18] AB Grudinin and S Gray. Passive harmonic mode locking in soliton fiber lasers. *JOSA B*, 14(1):144–154, 1997.

[19] J Nathan Kutz, BC Collings, K Bergman, and WH Knox. Stabilized pulse spacing in soliton lasers due to gain depletion and recovery. *IEEE journal of quantum electronics*, 34(9):1749–1757, 1998.

[20] D. Y. Tang, B. Zhao, D. Y. Shen, C. Lu, W. S. Man, and H. Y. Tam. Compound pulse solitons in a fiber ring laser. *Physical Review A*, 68(1):013816, July 2003.

[21] DY Tang, B Zhao, LM Zhao, and Hwa Yaw Tam. Soliton interaction in a fiber ring laser. *Physical Review E*, 72(1):016616, 2005.

[22] Veronika Tsatourian, Sergey V Sergeyev, Chengbo Mou, Alex Rozhin, Vitaly Mikhailov, Bryan Rabin, Paul S Westbrook, and Sergei K Turitsyn. Polarisation dynamics of vector soliton molecules in mode locked fibre laser. *Scientific reports*, 3(1):1–8, 2013.

[23] ZQ Wang, K Nithyanandan, A Coillet, P Tchofo-Dinda, and Ph Grelu. Optical soliton molecular complexes in a passively mode-locked fibre laser. *Nature communications*, 10(1):1–11, 2019.

[24] Andrey Komarov, Konstantin Komarov, and François Sanchez. Quantization of binding energy of structural solitons in passive mode-locked fiber lasers. *Physical Review A*, 79(3):033807, 2009.

[25] LM Zhao, DY Tang, Han Zhang, and X Wu. Bunch of restless vector solitons in a fiber laser with sesam. *Optics express*, 17(10):8103–8108, 2009.

[26] YF Song, H Zhang, LM Zhao, DY Shen, and DY Tang. Coexistence and interaction of vector and bound vector solitons in a dispersion-managed fiber laser mode locked by graphene. *Optics express*, 24(2):1814–1822, 2016.

[27] Chong Wang, Lu Wang, Xiaohui Li, Wenfeng Luo, Tianci Feng, Ying Zhang, Penglai Guo, and Yanqi Ge. Few-layer bismuthene for femtosecond soliton molecules generation in er-doped fiber laser. *Nanotechnology*, 30(2):025204, 2018.

[28] Chengbo Mou, Sergey V Sergeyev, Aleksey G Rozhin, and Sergei K Turitsyn. Bound state vector solitons with locked and precessing states of polarization. *Optics express*, 21(22):26868–26875, 2013.

[29] NN Akhmediev, A Ankiewicz, and JM Soto-Crespo. Stable soliton pairs in optical transmission lines and fiber lasers. *JOSA B*, 15(2):515–523, 1998.

[30] Ph Grelu, F Belhache, F Gutty, and J-M Soto-Crespo. Phase-locked soliton pairs in a stretched-pulse fiber laser. *Optics letters*, 27(11):966–968, 2002.

[31] MJ Lederer, Barry Luther-Davies, HH Tan, C Jagadish, NN Akhmediev, and JM Soto-Crespo. Multipulse operation of a ti: sapphire laser mode locked by an ion-implanted semiconductor saturable-absorber mirror. *JOSA B*, 16(6):895–904, 1999.

[32] Michel Olivier and Michel Piché. Origin of the bound states of pulses in the stretched-pulse fiber laser. *Optics express*, 17(2):405–418, 2009.

[33] Rafi Weill, Alexander Bekker, Vladimir Smulakovsky, Baruch Fischer, and Omri Gat. Noise-mediated casimir-like pulse interaction mechanism in lasers. *Optica*, 3(2):189–192, 2016.

[34] Jae K Jang, Miro Erkintalo, Stuart G Murdoch, and Stéphane Coen. Ultraweak long-range interactions of solitons observed over astronomical distances. *Nature Photonics*, 7(8):657–663, 2013.

[35] Wenbin He, Meng Pang, Dung-Han Yeh, Jiapeng Huang, CR Menyuk, and P St J Russell. Formation of optical supramolecular structures in a fibre laser by tailoring long-range soliton interactions. *Nature communications*, 10(1):1–9, 2019.

[36] Jose M Soto-Crespo, Nail Akhmediev, Ph Grelu, and F Belhache. Quantized separations of phase-locked soliton pairs in fiber lasers. *Optics letters*, 28(19):1757–1759, 2003.

[37] Yi Zhou, Yu-Xuan Ren, Jiawei Shi, Huade Mao, and Kenneth KY Wong. Buildup and dissociation dynamics of dissipative optical soliton molecules. *Optica*, 7(8):965–972, 2020.

[38] Luca Nimmesgern, Cornelius Beckh, Hannes Kempf, Alfred Leitenstorfer, and Georg Herink. Soliton molecules in femtosecond fiber lasers: universal binding mechanism and direct electronic control. *Optica*, 8(10):1334–1339, 2021.

[39] Kfir Sulimany, Ohad Lib, Gilad Masri, Avi Klein, Moti Fridman, Philippe Grelu, Omri Gat, and Hadar Steinberg. Bidirectional soliton rain dynamics induced by casimir-like interactions in a graphene mode-locked fiber laser. *Physical review letters*, 121(13):133902, 2018.

[40] Hendrik BG Casimir and Dirk Polder. The influence of retardation on the london-van der waals forces. *Physical Review*, 73(4):360, 1948.

[41] Rafi Weill, Alexander Bekker, Vladimir Smulakovsky, Baruch Fischer, and Omri Gat. Spectral sidebands and multipulse formation in passively mode-locked lasers. *Physical Review A*, 83(4):043831, 2011.

[42] Elham Nazemosadat and Arash Mafi. Nonlinear multimodal interference and saturable absorption using a short graded-index multimode optical fiber. *JOSA B*, 30(5):1357–1367, 2013.

[43] Fengyan Zhao, Hushan Wang, Yishan Wang, Xiaohong Hu, Ting Zhang, and Ran Pan. Observation of various bound states based on a graded index multimode fiber saturable absorber. *Laser Physics Letters*, 17(2):025105, 2020.

[44] Shijie Fu, Quan Sheng, Xiushan Zhu, Wei Shi, Jianquan Yao, Guannan Shi, Robert A Norwood, and N Peyghambarian. Passive q-switching of an all-fiber laser induced by the kerr effect of multimode interference. *Optics express*, 23(13):17255–17262, 2015.

[45] Huanhuan Li, Zhaokun Wang, Can Li, Junjie Zhang, and Shiqing Xu. Mode-locked tm fiber laser using smf-simf-gimf-smf fiber structure as a

saturable absorber. *Optics express*, 25(22):26546–26553, 2017.

[46] Zhaokun Wang, DN Wang, Fan Yang, Liujiang Li, Chunliu Zhao, Ben Xu, Shangzhong Jin, Shiying Cao, and Zhanjun Fang. Er-doped mode-locked fiber laser with a hybrid structure of a step-index–graded-index multimode fiber as the saturable absorber. *Journal of Lightwave Technology*, 35(24):5280–5285, 2017.

[47] Zhaokun Wang, DN Wang, Fan Yang, Liujiang Li, Chun-Liu Zhao, Ben Xu, Shangzhong Jin, Shi-Ying Cao, and Zhan-Jun Fang. Stretched graded-index multimode optical fiber as a saturable absorber for erbium-doped fiber laser mode locking. *Optics letters*, 43(9):2078–2081, 2018.

[48] Uğur Teğin and Bülend Ortaç. All-fiber all-normal-dispersion femtosecond laser with a nonlinear multimodal interference-based saturable absorber. *Optics letters*, 43(7):1611–1614, 2018.

[49] Fan Yang, DN Wang, Zhaokun Wang, Liujiang Li, Chun-Liu Zhao, Ben Xu, Shangzhong Jin, Shi-Ying Cao, and Zhan-Jun Fang. Saturable absorber based on a single mode fiber–graded index fiber–single mode fiber structure with inner micro-cavity. *Optics express*, 26(2):927–934, 2018.

[50] Tao Chen, Qiaoli Zhang, Yaping Zhang, Xin Li, Haikun Zhang, and Wei Xia. All-fiber passively mode-locked laser using nonlinear multimode interference of step-index multimode fiber. *Photonics Research*, 6(11):1033–1039, 2018.

[51] Fengyan Zhao, Ning Li, and Hushan Wang. Generation of a noise-like pulse from an erbium-doped fiber laser based on nonlinear multimode interference. *Laser Physics*, 30(12):125102, 2020.

[52] Fengyan Zhao, Hushan Wang, Xiaohong Hu, Yishan Wang, Wei Zhang, Ting Zhang, Chuandong Sun, and Zhijun Yan. Experimental observation of bound solitons with a nonlinear multimode interference-based saturable absorber. *Laser Physics Letters*, 15(11):115106, 2018.

[53] SMJ Kelly. Characteristic sideband instability of periodically amplified average soliton. *Electronics Letters*, 28(8):806–807, 1992.

[54] J. P. Gordon. Dispersive perturbations of solitons of the nonlinear Schrödinger equation. *Journal of the Optical Society of America B*, 9(1):91, January 1992.

[55] A.B. Grudinin, D.J. Richardson, and D.N. Payne. Energy quantisation in figure eight fibre laser. *Electronics Letters*, 28(1):67–68, January 1992.

[56] D. Y. Tang, L. M. Zhao, B. Zhao, and A. Q. Liu. Mechanism of multisoliton formation and soliton energy quantization in passively mode-locked fiber lasers. *Phys. Rev. A*, 72(4):043816, 2005.

[57] Rafi Weill, Boris Vodonos, Ariel Gordon, Omri Gat, and Baruch Fischer. Statistical light-mode dynamics of multipulse passive mode locking. *Physical Review E*, 76(3):031112, September 2007.

[58] Heman A Haus. Mode-locking of lasers. *IEEE Journal of Selected Topics in Quantum Electronics*, November/December 2000.

[59] H.A. Haus and A. Mecozzi. Noise of mode-locked lasers. *IEEE Journal of Quantum Electronics*, 29(3):983–996, March 1993.

[60] Michael Katz, Omri Gat, and Baruch Fischer. Noise-induced oscillations in fluctuations of passively mode-locked pulses. *Optics Letters*, 35(3):297–299, February 2010.